FLOW SOURCES AND FORMATION LAWS OF SOLAR WIND STREAMS

N. A. LOTOVA[1], V. N. OBRIDKO[1], K. V. VLADIMIRSKII[2], M. K. BIRD[3] and P. JANARDHAN[3,*]
[1]*IZMIRAN, Troitsk, Moscow Region, 142190, Russia (e-mail: nlotova@izmiran.troitsk.ru)*
[2]*Lebedev Physical Institute, Moscow, 117924, Russia*
[3]*Radioastronom. Institute, University of Bonn, 53121 Bonn, Germany*

(Received 14 March 2001; accepted 28 August 2001)

Abstract. The large-scale stream structure of the solar wind flow is studied in the main acceleration zone from 10 to 40 solar radii from the Sun. Three independent sets of experimental data were used: radio astronomical observations of radio wave scattering using the large radio telescopes of the Lebedev Physical Institute; dual-frequency Doppler solar wind speed measurements from the *Ulysses* Solar Corona Experiment during the spacecraft's two solar conjunctions in summer 1991 and winter 1995; solar magnetic field strength and configuration computed from Wilcox Solar Observatory data. Both the experimental data on the position of the transonic region of the solar wind flow and the solar wind speed estimates were used as parameters reflecting the intensity of the solar wind acceleration process. Correlation studies of these data with the magnetic field strength in the solar corona revealed several types of solar wind flow differing in their velocities and the location of their primary acceleration region.

1. Introduction

In spite of significant recent progress in understanding the solar wind, important problems such as the sources of the various types of streams and mechanisms of its acceleration remain unsolved. Furthermore, the problem has steadily become more complicated than presupposed. The acceleration mechanism had at one time been considered as a comparatively uncomplicated problem of spherically symmetric coronal expansion (Parker, 1958). After it was determined that the mean variation of the solar wind velocity field was of the order of the mean values (Armstrong and Woo, 1981; Scott, Coles, and Bourgois, 1983), a considerably more complicated mixed flow situation, where subsonic and supersonic streams coexist and interact, became apparent (Lotova *et al.*, 1995; Lotova, Blums, and Vladimirskii, 1985). As a consequence, recent theoretical and experimental efforts have focused on elucidating the sources and acceleration mechanisms of solar wind flows.

The spatial nonuniformity of the flow, manifested in the stream structure of the solar wind, and the associated sources of the solar wind in the corona have become of fundamental importance in the present problem of supersonic solar wind

[*]Now at Physical Research Laboratory, Ahmedabad 380 009, India.

Solar Physics **205:** 149–163, 2002.

formation. The large-scale structure of the flow in the main acceleration zone from 10 to 40 solar radii from the Sun is studied in this work. Noting that most of the acceleration zone is dominated by the magnetic energy density, data on the structure and intensity of the magnetic fields in the solar corona and their correlation with parameters of the flow are surely of prime importance. Such investigations have already been performed (Lotova, Obridko, and Vladimirskii, 2000, 2001), whereby the results of radio astronomical observations to determine the radial distance R_{in} of the inner boundary of the solar wind transonic region were correlated with coronal magnetic field data. Additional white-light coronagraph (WLC) data obtained from solar eclipses and SOHO observations were used to better define the solar wind flow structure in the discussion of these results.

Radio astronomical data are also used in the present paper. Moreover, a second, independent approach is provided by unique *Ulysses* results from the spacecraft's two solar conjunctions in summer 1991 and winter 1995. Dual-frequency Doppler observations were conducted and used to derive solar wind velocities V over the same range of radial distances investigated in the radio astronomical experiments. The use of these two data sets increases the reliability and broadens the applicability of the results.

2. Radio Astronomical Observations

Important results in the study of solar wind flow structure were obtained from observations of radio wave scattering in the circumsolar plasma. The solar occultations of compact natural sources such as quasars and water masers have been monitored regularly since 1987 with the large radio telescopes of the Lebedev Physical Institute at Pushchino (DCR-1000 at 103 MHz and RT-22 at 22.2 GHz). The observations and data processing methods are described elsewhere (Lotova, Blums, and Vladimirskii, 1985; Lotova, Rashkovetskii, and Kazimirskii, 1989; Lotova, 1988). These experiments revealed an extensive zone of enhanced scattering, which was identified with the (transonic) transition of the solar wind (Lotova, Blums, and Vladimirskii, 1985). Beginning in 1987, several sources were observed during conjunction at different solar distances and heliolatitudes either simultaneously or nearly simultaneously. The larger data volume enabled the construction of radio maps, i.e., two-dimensional projections of the transonic region in the plane of the sky (Lotova, Vladimirskii, and Korelov, 1997). Figures 1(a) and 1(b) show such radio maps for the data recorded in the years 1991 and 1995, respectively. For comparison, ground-based WLC eclipse images of the corona (negatives) are inserted at the position of the Sun. Figure 1(a) image was recorded during the solar eclipse of 12 July 1991 (Gulyaev and Philipov, 1992); Figure 1(b) image is dated 24 October 1995 (Rušin *et al.*, 1996). Deviations from spherical symmetry in Figures 1(a) and 1(b) are quite significant. Triangles denote the compact source 3C2 (March), circles represent the compact source in the Crab Nebula 3C144 and the quasars 3C133, 3C138, 3C152, 3C154, 3C166, 3C172, 3C208, 3C215, 3C225, 3C238 (June, August); squares are used for the quasars 3C245, 3C273, 3C275 and 3C279 (October); diamonds denote the masers S252A, GGD4 (June) and W31(2), IRC-20431 (December). The transonic region is hatched. Open symbols designate the inner boundary of the transonic region R_{in}; the solid symbols correspond to the outer boundary. As indicated in the two cases shown in Figure 1, the transonic region lies within the heliocentric radial distance range 10 $R_s < R <$ 40 R_s. The radio astronomical observations for these years can be compared immediately with the *Ulysses* velocity measurements.

The radio maps presented in Figures 1(a) and 1(b) already contain a considerable amount of information. It is obvious that the shape of the transonic region is far from being spherically symmetric. Its jagged boundaries imply a complicated solar wind stream structure. The radio maps do not give instantaneous representations of the transonic region shape, of course, because the zone changes as the data are accumulated over the course of the year. Nevertheless, the maps do provide a credible qualitative representation of the solar wind stream structure and its year-to-year changes. These changes are clearly seen in Figures 1(a) and 1(b). The transonic region moves closer to the Sun when proceeding from 1991 (year of maximum solar activity) to 1995 (year of solar minimum). A predominance of polar high-speed streams occurs in the epoch of solar minimum.

On the other hand, the radio maps say nothing about the details of the process, the solar wind sources, the acceleration control factors, or the role of the stream structure. We consider these problems below by discussing the correlative relations between the radial distance R_{in} of the inner boundary of the solar wind transonic region and the results of solar wind velocity measurements with magnetic field estimates in the solar corona, i.e., at the bottom of the zone of the primary solar wind acceleration.

3. *Ulysses* Velocity Measurements

Extensive dual-frequency (S- and X-band) ranging and Doppler observations were conducted in support of the *Ulysses* Solar Corona Experiment (SCE) during the spacecraft's solar conjunctions in summer 1991 (C_1) and winter 1995 (C_4). Tracking was performed on a nearly continuous basis by the NASA Deep Space Network (DSN). While the ray path from *Ulysses* to Earth was always close to the ecliptic during the conjunction in August–September 1991 (Bird *et al.*, 1994), it passed through all heliolatitudes from South Pole to equator at distances between 20–30 R_s during the conjunction in February–March 1995 (Bird *et al.*, 1996). This work utilizes the results of a two-station cross-correlation analysis of dual-frequency Doppler measurements to determine coronal plasma velocities during both C_1 and C_4 (Janardhan *et al.*, 1999).

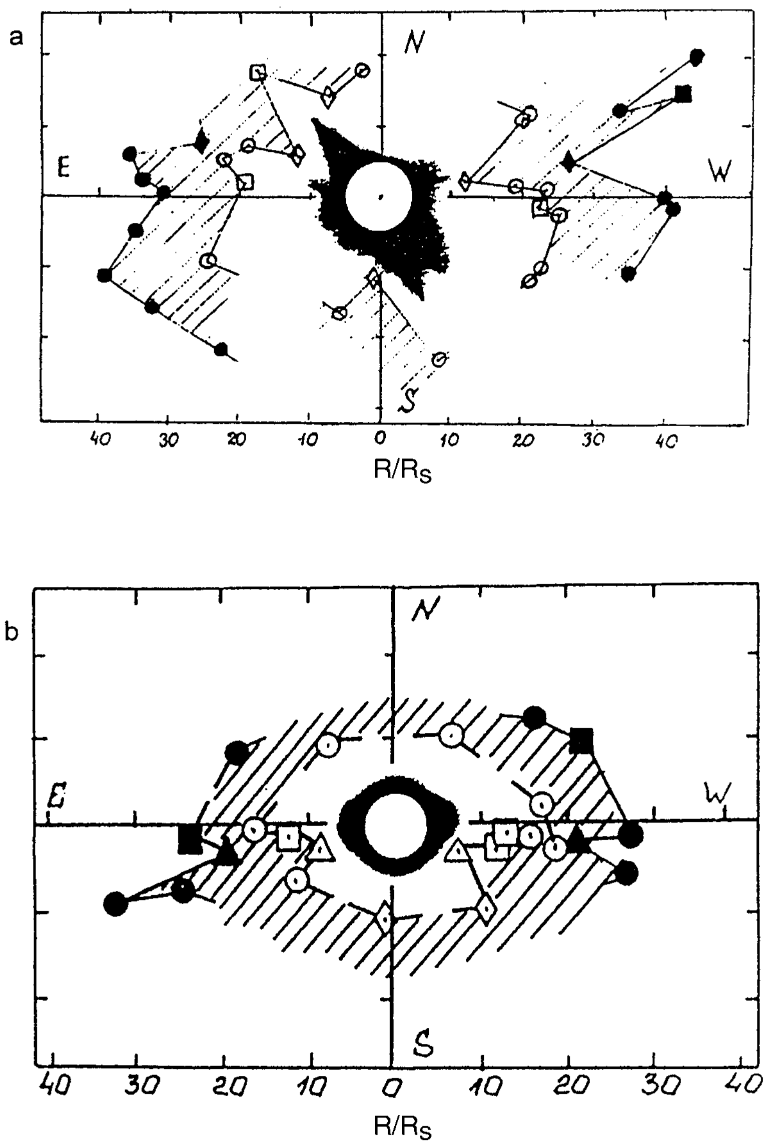

Figure 1. Radio maps of the solar wind transonic region: (a) 1991 – solar maximum, (b) 1995 – solar minimum. Ground-based WLC eclipse images of the corona (negatives) on 12 July 1991 (Gulyaev and Philipov, 1992) and 24 October 1995 (Rušin *et al.*, 1996) are centered on the Sun. The various symbols denoting the boundaries of the transonic region are given in the text and Tables I and III. *Open* (*solid*) symbols denote the inner (outer) boundary of the transonic region.

The inhomogeneities of the intervening coronal plasma produce frequency dependent variations in the phase velocity of the two received carrier frequencies. The coronal signature can be isolated from other Doppler variations (e.g., from the trajectory) by calculating a differenced quantity, the 'differential Doppler residual', which is proportional to the time derivative of the electron column density along the ray path from *Ulysses* to Earth.

Ulysses Doppler data were sometimes recorded simultaneously at different ground stations. On many of these occasions it was possible to perform a cross-correlation analysis with the overlapping data from the two stations. The time lag of maximum correlation was assumed to be the time taken for the solar wind to move a distance equal to the radial projection ΔR of the spatial separation of the radio ray paths between the two ground stations and *Ulysses*. Typical values for ΔR are a few thousand km. The raw measurements of Doppler residuals at each ground station were recorded at a sample rate of 1 Hz. A filtering technique was applied to enhance the correlations. Roughly half of the original two-station data sets exhibited correlations greater than 0.4 and were used for this analysis (Janardhan *et al.*, 1999).

4. Solar Coronal Magnetic Fields

As stated above, the information on the solar wind sources and the factors determining the acceleration process were obtained from a correlation between the experimental data (R_{in} and V), and the calculated parameters of the solar corona magnetic fields. For the latter, the magnetic field calculations are also based on experimental data, optical measurements of magnetic fields at the photospheric level recorded at the Wilcox Solar Observatory (WSO), Stanford University (*http://quake.stanford.edu/wso/wso.html*). These data are used as a lower boundary condition for computation of the potential field solution from the Maxwell equations for the region $R_s \leq R \leq 2.5\ R_s$ (Hoeksema, Wilcox, and Scherrer, 1982, 1983; Hoeksema and Scherrer, 1986; Obridko and Shelting, 1999a).

Calculation of the magnetic field in the solar environment is no easy task. Many methods are available for extrapolating the field above the photosphere, where, in fact, the measurements are taken. Best known are the methods developed at Stanford and described in detail in publications of the Stanford team. All of them have their merits and drawbacks. All methods use potential approximation but differ somewhat as to allowance for the field at high heliographic latitudes.

We have used here the so-called classical method, where the field is assumed to be potential everywhere including the boundary surfaces, the source surface is at 2.5 solar radii, and a special polar correction is performed. It should be noted that we used only initial Internet data and re-calculated all coefficients using an original program partly described in Obridko and Shelting (1999a). In the same work, it is shown that our results agree fairly well with those obtained from the classical WSO coefficients.

The disadvantages of the classical method are well known. It does not always provide good agreement with the interplanetary field measured at the Earth's orbit, as shown, in particular, by Obridko, Kharshiladze, and Shelting (1995, 1996), and Obridko and Shelting (1998). However, this disagreement seems to be due to the processes in interplanetary space, while the field in the vicinity of the Sun is quite adequately calculated by the classical method. It is better than other methods in describing the location of the heliomagnetic equator, sector structures, coronal rays, and streamers, which is corroborated both by eclipse topological data and by non-eclipse Hα observations (Sýkora *et al.*, 1998, 1999; Sýkora, Badalyan, and Obridko, 2001b; Obridko and Shelting, 1999a – correlation with the IMF sign; Ivanov *et al.*, 1999 – CME location; Obridko and Shelting, 1992a, 1999b; Sýkora, Badalyan, and Obridko, 2001 – comparison of open field lines and coronal holes; Obridko and Shelting, 1992b – cyclic variations in global indices; Badalyan, Obridko, and Sýkora, 1999 – comparison with the green line polarization in the corona). Thus, the classical method can well be applied, particularly, for statistical calculations.

Of course, our calculations provide but a mere indication (sometimes pretty rough) to the existence of specific features in the solar wind. In the future, our results will, obviously, be ascertained by finer methods and direct observations. In this context, we pin our hopes on the *Solar Orbiter* mission, which is supposed to conduct direct measurements in the region of space we are interested in.

The results of magnetic field calculations are presented in two forms. First, absolute values of the radial component of the magnetic field $|B_R|$ were calculated for $R = 2.5\ R_s$. The radial distance 2.5 R_s was assumed to be the source surface, the starting height for the solar wind acceleration process. The time (transformed to Carrington longitude) and solar disk position angle (transformed to heliographic latitude) coordinates for the calculations of B_R were chosen such that they lie on the same solar wind streamline mapped radially downward from the ray path proximate point corresponding to the measured values of R_{in} or V.

The second form, a very important one because it gives the field topology in the solar wind's source region, was also derived from WSO data. The field line topology was constructed using a uniform network of points on the solar surface ($R = 1\ R_s$), as footpoints. With the magnetic field components calculated under the potential approximation and the above-mentioned limitations taken into account, one can readily trace the field lines originating from a given uniform grid on the photosphere. The distance between the grid nodes is chosen depending on the complexity of the structure under consideration. The calculated topology of the field lines is usually checked by independent direct observations of the corona using eclipse or satellite techniques. These magnetic topology diagrams are quite complicated and difficult to interpret. Nevertheless, they reveal some important types of magnetic field structure: an open field type with field lines extending into

TABLE I

Solar wind flow structures from radio astronomy sounding and magnetic data for 1991.

No.	Source	Symbol in Figure 1(a)	1991 date	E/W	φ deg	R_{in} R_s	$\lvert B_r \rvert$ μT	Magnetic field structure B_r
1	3C279	square	3 Oct.	E	4	19	1.65	Open
2	3C238	circle	24 Aug.	E	−70	17	3.17	
3	IRC-20431	diamond	20 Dec.	E	25	15	3.88	
4	W31(2)	diamond	22 Dec.	E	63	16	4.96	
5	S252A	diamond	23 June	E	−87	∼10	7.95	
6	GGD4	diamond	20 June	W	16	12	9.18	
7	3C138	circle	13 June	W	−71	24	3.98	Closed
8	3C154	circle	1 July	W	30	23	4.07	
9	3C245	square	30 Sept.	E	81	18	11.67	
10	3C144	circle	22 June	W	−4	25	5.90	Mixed
11	3C273	square	24 Sept.	E	46	25	7.61	
12	3C166	circle	26 June	E	−21	25	8.02	
13	3C152	circle	22 June	W	−23	23	9.32	
14	3C279	square	15 Oct.	W	−3	22	9.98	
15	3C133	circle	14 June	W	30	24	10.56	
16	3C133	circle	2 June	E	16	23	14.01	
17	3C225	circle	22 Aug.	W	3	23	14.02	
18	3C208	circle	10 Aug.	W	−27	24	15.20	
19	3C215	circle	11 Aug.	W	6	19	15.94	
20	3C172	circle	1 July	E	20	21	16.10	

space, a closed type with loop structures, and a mixed case, which is a broadly spread combination of the two previous types.

5. Basic Results

A total of 69 data set pairs were obtained in the two years 1991 and 1995, thereby enabling investigations of the correlations of R_{in} or V with $|B_R|$ at two very different epochs of the solar activity cycle. These data are presented in Tables I–IV, divided according to year and method of observation. Tables I and III present the R_{in}, $|B_R|$pairs; Tables II and IV show the V, $|B_R|$data.

Tables I and III give the date of observation, name of the occulted source and coordinates of the inner boundary of the transonic region R_{in}, E/W solar limb, heliolatitude, and radial distance from the Sun. Tables II and IV contain the date and

TABLE II

Solar wind flow structures from *Ulysses* radio sounding and magnetic data for 1991.

No.	1991 date	E/W	R R_S	φ deg	V km s^{-1}	$\pm\Delta V$ km s^{-1}	$\|B_R\|$ μT	Magnetic field structure B_R
1	12 Aug.	E	23.3	8	262	51	0.77	Open
2	12 Aug.	E	22.3	9	257	21	0.62	
3	11 Aug.	E	26.6	7	206	11	0.33	
4	11 Aug.	E	26.5	7	218	28	0.33	
5	25 Aug.	W	12.2	23	276	12	2.31	
6	17 Aug.	E	9.6	24	331	49	6.26	
7	1 Sept.	W	28.9	10	451	64	10.21	
8	2 Sept.	W	31.8	10	413	73	11.69	
9	11 Aug.	E	26.5	7	118	40	0.33	Closed
10	10 Aug.	E	26.6	7	121	2	3.94	
11	3 Sept.	W	34.5	9	269	47	12.34	
12	30 Aug.	W	24.4	12	49	1	1.34	Mixed
13	27 Aug.	W	18.5	15	41	1	1.89	
14	18 Aug.	E	7.4	33	30	0.5	10.51	
15	4 Sept.	W	37.8	8	101	20	13.02	
16	12 Aug.	E	22.2	9	346	36	0.62	Complex
17	12 Aug.	E	22.2	9	425	56	0.62	
18	16 Aug.	E	12.1	19	518	72	0.13	
19	16 Aug.	E	12.0	19	519	95	0.13	

ray path proximate point coordinates associated with the velocity measurements and the corresponding standard error. All tables give the field strength $|B_R|$ at the source surface $R = 2.5\ R_s$ and are ordered according to the magnetic field topology data: open, closed, or mixed type.

The correlations between the flow parameters and magnetic field data cannot be perceived from the tables alone. Figures 2–5 present the data from Tables I–IV in graphical form. Taking into account the magnetic topology data, it becomes apparent that distinct correlation relations exist and fall into some separate branches on each diagram. Separate types of solar wind flows correspond to each of these branches, differing by the source conditions and acceleration progress.

Figures 2 and 3, which show the 1991 results, exhibit a comparatively simple situation corresponding to the phase of maximum solar activity. Three types of field are seen on both diagrams. Triangles represent high-speed flows emerging from the periphery of a streamer – a previously unknown type of high-speed flow. Com-

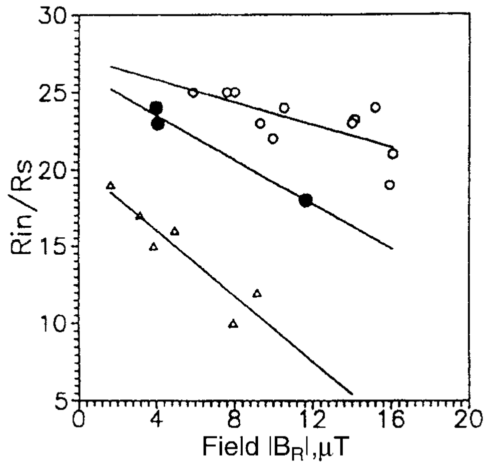

Figure 2. Correlation diagram for 1991. Position of the inner boundary of the transonic region R_{in} vs. magnetic field $|B_R|$. *Triangles* denote the high-speed solar wind component with open magnetic field lines; *solid circles* correspond to the slow-speed solar wind above closed magnetic field structures; *open circles* represent the slowest solar wind component associated with mixed magnetic field structures.

TABLE III

Solar wind flow structures from radio astronomy sounding and magnetic data for 1995.

No.	Source	Symbol in Figure 1(b)	1995 date	E/W	φ deg	R_{in} R_S	$\|B_R\|$ μT	Magnetic field structure B_R
1	3C279	square	18 Oct.	W	−3	13.5	0.88	Open – weak B_R
2	3C275	square	8 Oct.	W	−9	13.0	1.37	
3	3C144	circle	12 June	E	30	13.0	1.54	
4	3C275	square	1 Oct.	E	−3	12.0	1.50	
5	3C2	triangle	20 March	E	−17	9.0	0.92	
6	3C2	triangle	24 March	W	−17	8.0	3.25	
7	3C154	circle	27 June	W	55	12.0	6.06	Open – strong B_R
8	3C154	circle	23 June	E	49	12.0	7.55	
9	S252A	diamond	23 June	E	−87	10.5	12.90	
10	S252A	diamond	26 June	W	−40	14.5	3.80	Closed
11	3C225	circle	21 Aug.	W	3	16.0	0.85	
12	3C225	circle	11 Aug.	E	−2	16.5	0.07	
13	3C215	circle	11 Aug.	W	5	17.0	0.38	
14	3C144	circle	20 June	W	−7	19.0	0.96	

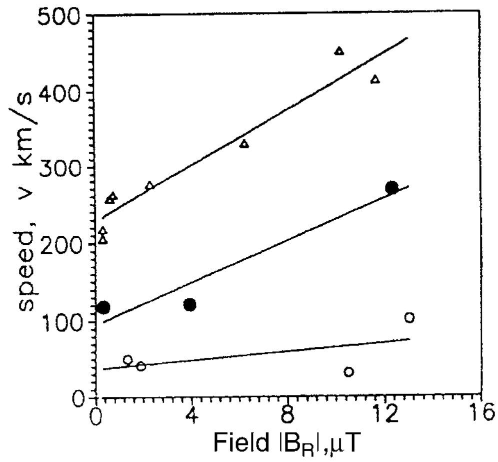

Figure 3. Correlation diagram for 1991. Solar wind velocity V vs. magnetic field $|B_R|$. The symbols are defined in the caption to Figure 2.

parison with the WLC structure observed by SOHO-LASCO shows that this type of magnetic field structure corresponds to the lateral lobe of a streamer (Lotova, Obridko, and Vladimirskii, 2000, 2001). Streamers have not been generally considered among the possible sources of high-speed solar wind flows (Schwenn, 1983, 1990). Solid circles represent low-speed streams embedded in the main body of a streamer – a well-known type (Koutchmy, 1988; Koutchmy and Livshits, 1992). These flow types can also be quickly identified from the morphology observed by the SOHO-LASCO WLC (Lotova, Obridko, and Vladimirskii, 2000, 2001). Open circles denote the slowest solar wind type, also as yet unknown. The line of sight for these measurements passed through an extensive region of amorphous luminosity as observed by SOHO-LASCO (Lotova, Obridko, and Vladimirskii, 2000, 2001).

An important result of this analysis is that distinct types of magnetic field structure correspond to different types of solar wind streams. The high-speed flows arise from the open magnetic field areas of the solar corona, while the slow-speed flows correspond to closed or mixed types of magnetic structures. This latter type, marked with open circles in the above figures, evidently occupies large areas of the source surface. It is noted that Table II also contains some drastic deviations from the above correlations. The last four entries in this table are for solar wind streams combining high ($\sim$350–500 km s^{-1}) velocities with very low magnetic field strength in their source area. These sources are identified here as local coronal holes with a very complicated magnetic field structure. The flows implied by these data may be associated with nonstationary processes falling outside the limits of quiet Sun conditions. The corresponding data points are not plotted in Figure 3.

Figures 4 and 5 illustrate the data for 1995, i.e., a year of solar minimum. The differences compared to 1991 are quite pronounced. Figure 4 again shows three separate correlation branches. The branch marked with triangles corresponds to the

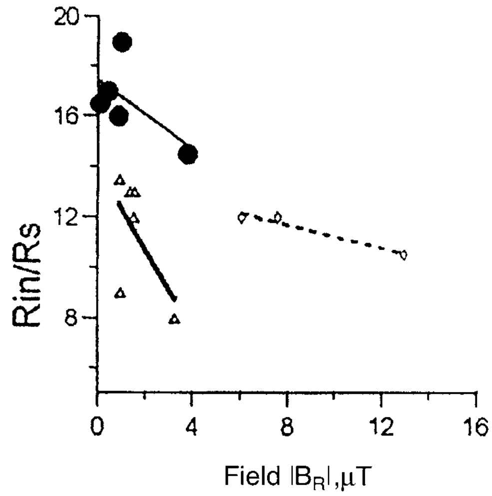

Figure 4. Correlation diagram for 1995. R_{in} vs magnetic field $|B_R|$. *Diamonds* mark the high-speed solar wind component with a very high magnetic field strength in an open field line configuration. See Figure 2 for the definition of other solar wind flow types.

same type of high-speed streams known from the 1991 results. The sources here are again peripheral channels of coronal streamers. The branch marked with solid circles is connected with the main body of streamers. A new branch, marked with diamonds, is connected with polar coronal holes (Krieger, Timothy, and Roelef, 1973; Timothy, Krieger, and Vaiana, 1975; Schwenn, 1983, 1990). The source regions are characterized by strong magnetic fields. We thus see two types of high-speed streams in Figure 4, differing by the type of source. Conspicuous at solar minimum is the absence of the slowest type of streams (marked with open circles in Figures 2 and 3) connected with the mixed type of magnetic field structure.

Figure 5 presents results based on the *Ulysses* SCE solar wind velocity measurements (Janardhan *et al.*, 1999). The case statistics for high-speed streams (denoted by triangles) is sparse. In this case they are connected with local coronal holes (entries 7–9 in Table IV). The second type of the high-speed streams, connected with polar coronal holes, is also present in Table IV (last 6 entries). Exceptionally high velocities (1000 to 2500 km s^{-1}) were derived for these streams. Because velocities so large are very seldom measured in polar coronal holes at solar minimum (Phillips *et al.*, 1995), it is likely that they are the result of unfavorable projection effects. These results are not included in Figure 5. It is noted that Grall *et al.* (1996) also derive very high velocities from interplanetary scintillation measurements in polar coronal holes.

Low-speed streams in the main body of streamers (solid circles) are also illustrated in Figures 4 and 5. These data are rather sparse and provide poor statistics. Contrary to Figure 4, several points corresponding to the slowest streams, broadly

TABLE IV

Solar wind flow structures from *Ulysses* radio sounding and magnetic data for 1995

No.	1995 date	E/W	R R_s	φ deg	V km s^{-1}	$\pm\Delta V$ km s^{-1}	$\|B_r\|$ μT	Magnetic field structure B_R
1	8 March	SW	26.2	−12	431	93	0.54	Open – weak B_R
2	8 March	SW	26.2	−12	346	51	0.54	
3	8 March	SW	26.5	−11	356	41	0.54	
4	7 March	SW	25.1	−16	287	28	0.56	Closed
5	10 March	SW	29.7	−4	210	18	2.13	
6	11 March	SW	30.4	−2	216	39	2.14	
7	9 March	SW	27.2	−10	96	8	1.31	Mixed
8	1 March	SW	21.7	−56	184	23	8.69	
9	2 March	SW	21.4	−50	140	22	7.75	
10	3 March	SW	21.5	−43	194	41	7.17	
11	22 March	SE	29.6	−88	2573	1073	12.33	Open – strong B_R
12	23 March	SE	27.9	−88	1382	466	12.29	
13	24 March	SE	26.4	−84	1659	593	12.24	
14	25 Febr.	SW	25.1	−79	1326	472	12.08	Complex
15	27 Febr.	SW	22.9	−69	1009	305	10.36	
16	8 March	SW	26.2	−12	936	417	0.54	

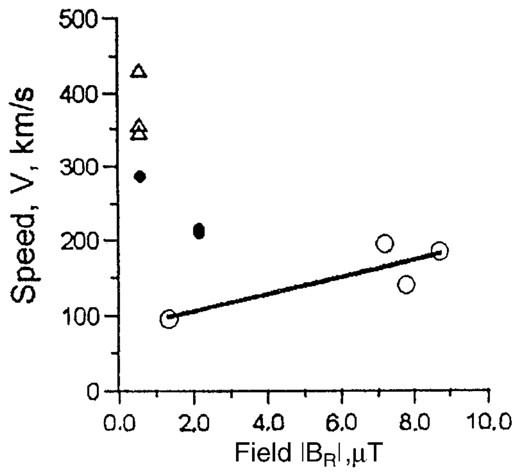

Figure 5. Correlation diagram for 1995. Solar wind velocity V vs. magnetic field $|B_R|$. The symbols are defined in the caption to Figure 2.

present in the 1991 results, were obtained in Figure 5 (open circles), thereby confirming the presence of this component in 1995.

From the above analysis it may be concluded that four different stream types are revealed in the solar wind flow. The four branches of the above described correlations correspond to these stream types, each of which originates in areas of the solar corona differing by their magnetic field strength and structure.

As mentioned above, comparison of the radio maps for 1991 and 1995 (Figures 1(a) and 1(b)) provides important information on the solar wind flow evolution over the course of the 11-year cycle. Nevertheless, important details of the mechanism remain unclear. The present results elucidate some of these problems. The very existence of different solar wind stream types implies that the different acceleration processes are governed by the parameters of the magnetic fields in the coronal source region. It follows that the changes of the solar wind flow over the course of the 11-year cycle are changes of the relative numbers of the different stream types, changing with the changing statistics of the magnetic field structures in their solar coronal origin. During years of maximum solar activity, closed or mixed magnetic structures and slow solar wind streams dominate. In epochs of minimum activity, the magnetic structures are mostly of an open type and generate fast solar wind streams.

6. Conclusions

Two different radio occultation methods were utilized for a coordinated investigation of the solar wind acceleration at solar offset distances from 10 to 40 R_s: the traditional radio astronomical determination of the inner boundary of the transonic region R_{in} and the unique *Ulysses* SCE measurements of solar wind velocity V. Both of these data sets were correlated with derivations of magnetic field strength $|B_R|$ on a source surface at 2.5 R_s, in the region of the solar wind flow sources.

The correlation diagrams revealed several branches of correlative interdependence and, as a corollary, several types of solar wind streams. The different types of streams correlate with different types of magnetic field topology in the solar wind source area. A total of four specific types, two of high-speed and two of low-speed, were revealed.

Both high-speed components are associated with open, but slightly different, magnetic field configurations in the corona. One type, known earlier, emanates from polar coronal holes, i.e., regions of very strong magnetic field. The second stream type, revealed in the present work, originates from the periphery of the adjacent streamer structure. The magnetic parameters and structure of these two types are similar to the familiar stream type coming from local coronal holes.

The two low-speed solar wind stream types also differ by their associated magnetic field structure near their origin. The previously known stream type, contained within the main body of coronal streamers, is associated with a closed, loop-like magnetic field topology. Streams of the second type, which are characterized by the lowest measured velocities, originate in extensive areas of the solar corona with mixed magnetic field structure where loop field line structures are interspersed with field lines extending out into interplanetary space. Following earlier work (Lotova, Obridko, and Vladimirskii, 2000, 2001), the results of the present paper further elucidate the salient features of solar wind flow evolution over the course of the 11-year solar activity cycle. The fundamental element here is the evolution of the magnetic fields in the solar corona. Mixed-type magnetic field structures and the slowest solar wind streams prevail in the years near solar maximum. During the solar minimum epoch, however, open-type magnetic fields and, accordingly, high-speed solar wind streams are predominant.

Acknowledgements

The authors are extremely grateful to the staff of the Wilcox Solar Observatory for providing solar magnetic field data on their website. The work was sponsored by the Russian Foundation for Basic Research (RFBR), grant 01-02-16308, the joint project RFBR-DFG (Deutsche Forschungsgesellschaft), grant 00-02-04022 G, the Russian Federal Astronomy Program, the INTAS project, grant 97-02-71032, and by the Russian Program of Leading Scientific Schools, project 00-15-96661.

References

Armstrong, J. W. and Woo R.: 1981, *Astron. Astrophys.* **103**, 415.

Badalyan, O. G., Obridko, V. N., and Sýkora, J.: 1999, in K. N. Nagendra and J. O. Stenflo (eds.), *Proceedings SPW2, Solar Polarization*, Kluwer Academic Publishers, Dordrecht, p. 373.

Bird, M. K., Volland, H., Pätzold, M., Edenhofer, P., Asmar, S. W., and Brenkle, J. P.: 1994, *Astrophys. J.* **426**, 373.

Bird, M. K., Pätzold, M., Edenhofer, P., Asmar, S. W., and McElrath, T. P.: 1996, *Astron. Astrophys.* **316**, 441.

Grall, R. R., Coles, W. A., Klinglesmith, M. T. *et al.*: 1996, *Nature* **379**, 429.

Gulyaev, R. A. and Philipov, B. P.: 1992, *Dokl. RAS* **322**, 268.

Hoeksema, J. T. and Scherrer, P. H.: 1986, *Solar Magnetic Field – 1976 through 1985*, WCDA, Boulder, CO, U.S.A.

Hoeksema, J. T., Wilcox, J. M., and Scherrer, P. H.: 1982, *J. Geophys. Res.* **87**, 10331.

Hoeksema, J. T., Wilcox, J. M., and Scherrer, P. H.: 1983, *J. Geophys. Res.* **88**, 9910.

Ivanov, E. V., Obridko, V. N., Nepomnyashchaya, E. V, and Kutilina, N. V: 1999, *Solar Phys.* **184**, 369.

Janardhan, P., Bird, M. K., Edenhofer, P., Wohlmuth, R. Plettemeier, D., Asmar, S. W., Pätzold, M., and Karl, J.: 1999, *Solar Phys.* **184**, 157.

Koutchmy, S.: 1988, *Space Sci. Rev.* **47**, 95.

Koutchmy, S. and Livshits, M.: 1992, *Space Sci. Rev.* **61**, 393.

Krieger, A. S., Timothy, A. F., and Roelef, E. C.: 1973, *Solar Phys.* **23**, 123.

Lotova, N. A.: 1988, *Solar Phys.* **117**, 399.

Lotova, N. A., Blums, D. F., and Vladimirskii, K. V.: 1985, *Astron. Astrophys.* **150**, 266.

Lotova, N. A., Obridko, V. N., and Vladimirskii, K. V.: 2000, *Astron. Astrophys.* **357**, 1051.

Lotova, N. A., Obridko, V. N., and Vladimirskii, K. V.: 2001, *Astron. Zh.* (in press).

Lotova, N. A., Rashkovetskii, A. A., and Kazimirskii, P. B.: 1989, *Astron. Zh.* **66**, 114.

Lotova, N. A., Vladimirskii, K. V., and Korelov, O. A.: 1997, *Solar Phys.* **172**, 225.

Lotova, N. A., Vladimirskii, K. V., Yurovskaya, I. Y., and Korelov, O. A.: 1995, *Astron. Zh.* **72**, 757.

Obridko, V. N. and Shelting, B. D.: 1998, *Advances in Solar Connection with Interplanetary Phenomena, Proceedings of the third SOLTIP Symposium*, Beijing, China, October 14–18, 1996, Beijing, p. 447.

Obridko, V. N. and Shelting, B. D.: 1999a, *Solar Phys.* **184**, 187.

Obridko, V. N. and Shelting, B. D. : 1999b, *Solar Phys.* **187**, 185.

Obridko V. N., Kharshiladze, A. F. and Shelting, B. D.: 1995, *Proceedings of the Second SOLTIP Symposium*.

Obridko, V. N., Kharshiladze, A. F., and Shelting, B. D.: 1996, in: K. S. Balusubramaniam, Stephen Keil and Raymond N. Smart (eds.), *Solar Drivers of Interplanetary and Terrestrial Disturbances, ASP Conference Series*, **95**, 366.

Obridko, V. N. and Shelting, B. D.: 1992a, in K. L. Harvey (ed.), *The Solar Cycle. Proceedings of the National Solar Observatory /Sacramento Peak 12 Summer Workshop*, **27**, 187.

Obridko, V. N. and Shelting, B. D.: 1992b, *Solar Phys.* **137**, 167.

Parker, E. N.: 1958, *Astrophys. J.* **128**, 664.

Phillips, J. L., Bame, S. J., Barnes, A. *et al.*: 1995, *Geophys. Res. Lett.* **22**, 3301.

Rušin, V., Klocok, L., Minarovjech, M., and Rybanský, M.: 1996, *Contrib. Astron. Observ. Skalnaté Pleso* **26**, 37.

Scott, S. I., Coles, W. A., and Bourgois, G.: 1983, *Astron. Astrophys.* **123**, 207.

Schwenn, R.: 1983, in M. Neugebauer (ed.), *Solar Wind 5, NASA Conf. Publ.* **2280**, 489.

Schwenn, R.: 1990, in R. Schwenn and E. Marsch (eds.), *Physics of the Inner Heliosphere*, Springer-Verlag, Heidelberg, p. 99.

Sýkora, J., Badalyan, O. G., and Obridko, V. N.: 2001a, in A. Wilson (ed.), *The Solar Cycle and Terrestrial Climate*, ESA SP-463 (in press).

Sýkora, J., Badalyan, O. G., and Obridko, V. N.: 2001b, *Adv. Space Res.* (in press).

Sýkora, J., Ambrož, P., Minarovjech, M., Obridko, V. N., Pinter, T., and Rybanský, M.: 1998, *Solar Jets and Coronal Plumes. Proceedings of an International Meeting* held in Guadeloupe, DOM, France, 23–26 February 1998, ESA SP-421, p. 79.

Sýkora, J., Badalyan, O. G., Obridko, V. N., and Pinter, T.: 1999, *Contrib. Astron. Observ. Skalnaté Pleso* **29**, 89.

Timothy, A. F., Krieger, A. S., and Vaiana, G. S.: 1975, *Solar Phys.* **42**, 135.